

# Ab initio High-throughput screening of transition metal double chalcogenide monolayers as highly efficient bifunctional catalysts for photochemical and photoelectrochemical water splitting

Linlin Liu,<sup>a,b</sup> Bowen Jiang,<sup>a,b,c</sup> Dan Sun,<sup>b,d</sup> Hanyu Liu,<sup>a,b,c,e</sup> Yu Xie,<sup>\*a,b,e</sup>

## 1 Structural information, the energy above convex hull and the heat of formation of 2D MXY

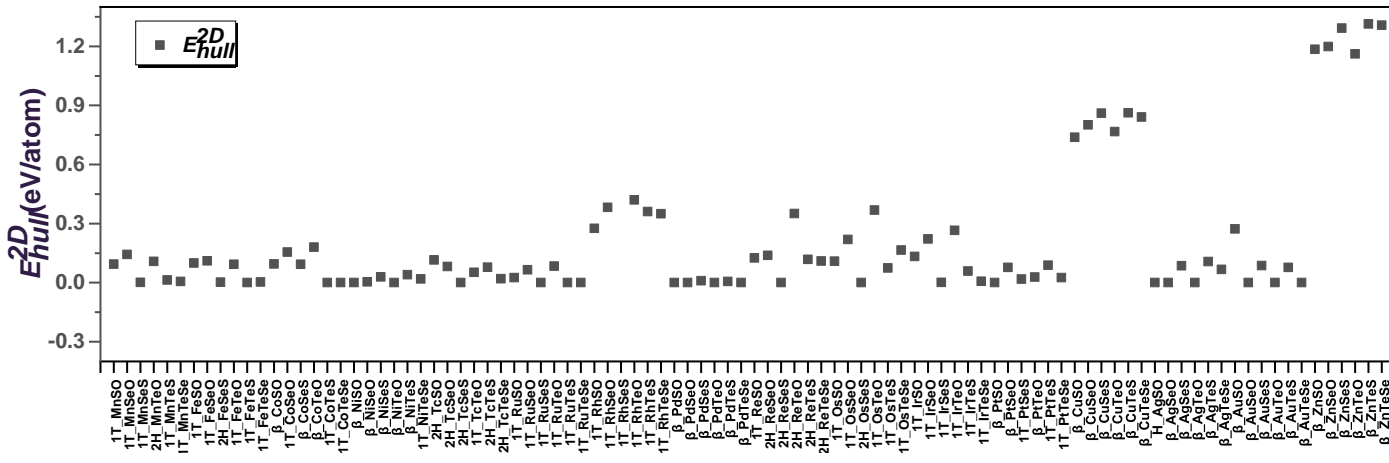


Fig. S1 The energy above convex hull ( $E_{\text{hull}}$ ).

Considering recent rapid developments in growing few-layer 2D crystals, the heat of formation of the 384 monolayer TMXY in the relaxed structure was calculated from  $E_{\text{form}}(\text{MXY}) = 1/3E_{\text{tot}}(\text{MXY}) - E(\text{M}) - E(\text{X}) - E(\text{Y})$ , where  $E_{\text{tot}}(\text{MXY})$  is the PBE total energy of the monolayer and  $E(\text{TM})$ ,  $E(\text{X})$  and  $E(\text{Y})$  are the energies of the metal and chalcogen (X and Y), respectively. The energy convex hull describes the competition between all different phases with the same compositions.

Table S1 Optimized lattice constants( $a$  and  $b$ ), bond length( $d_{\text{M-X/Y}}$ ), vertical height( $h$ ). The lattice parameters are given in Angstrom. Calculated heat of formation  $E_{\text{form}}$  for all monolayers. The unit is eV.

Materials	$a$	$b$	$d_{\text{M-X/Y}}$	$h$	$E_{\text{form}}$
$\beta$ _NiSO	4.91	4.85	1.96/2.09	1.33	-0.62
$\beta$ _NiSeO	5.08	5.03	2.23/1.92	1.53	-0.53
$\beta$ _NiSeS	5.52	5.37	2.30/2.17	1.38	-0.32
$\beta$ _NiTeO	5.32	5.22	2.40/1.94	1.75	-0.68
$\beta$ _NiTeS	5.79	5.59	2.46/2.19	1.34	-0.27
$\beta$ _PdSO	5.14	5.15	2.24/2.16	0.95	-0.45
$\beta$ _PdSeO	5.38	5.3	2.36/2.15	1.4	-0.49
$\beta$ _PdTeO	5.62	5.49	2.52/2.18	1.61	-0.53
$\beta$ _PdTeS	6.01	5.82	2.60/2.37	1.65	-0.37
$\beta$ _PdTeSe	6.17	5.94	2.59/2.48	1.6	-0.40
$\beta$ _PtSO	5.17	5.13	2.23/2.15	1.22	-0.54
$\beta$ _PtSeO	5.34	5.29	2.35/2.14	1.43	-0.47
$\beta$ _PtTeO	5.58	5.47	2.51/2.17	1.65	-0.51
1T_PtTeS	3.81	3.81	2.63/2.50	2.62	-0.24
1T_PtTeSe	3.89	3.89	2.65/2.59	2.7	-0.35

<sup>a</sup>State Key Laboratory of Superhard Materials, College of Physics, Jilin University, Changchun, 130012, China; E-mail: xieyu@jlu.edu.cn

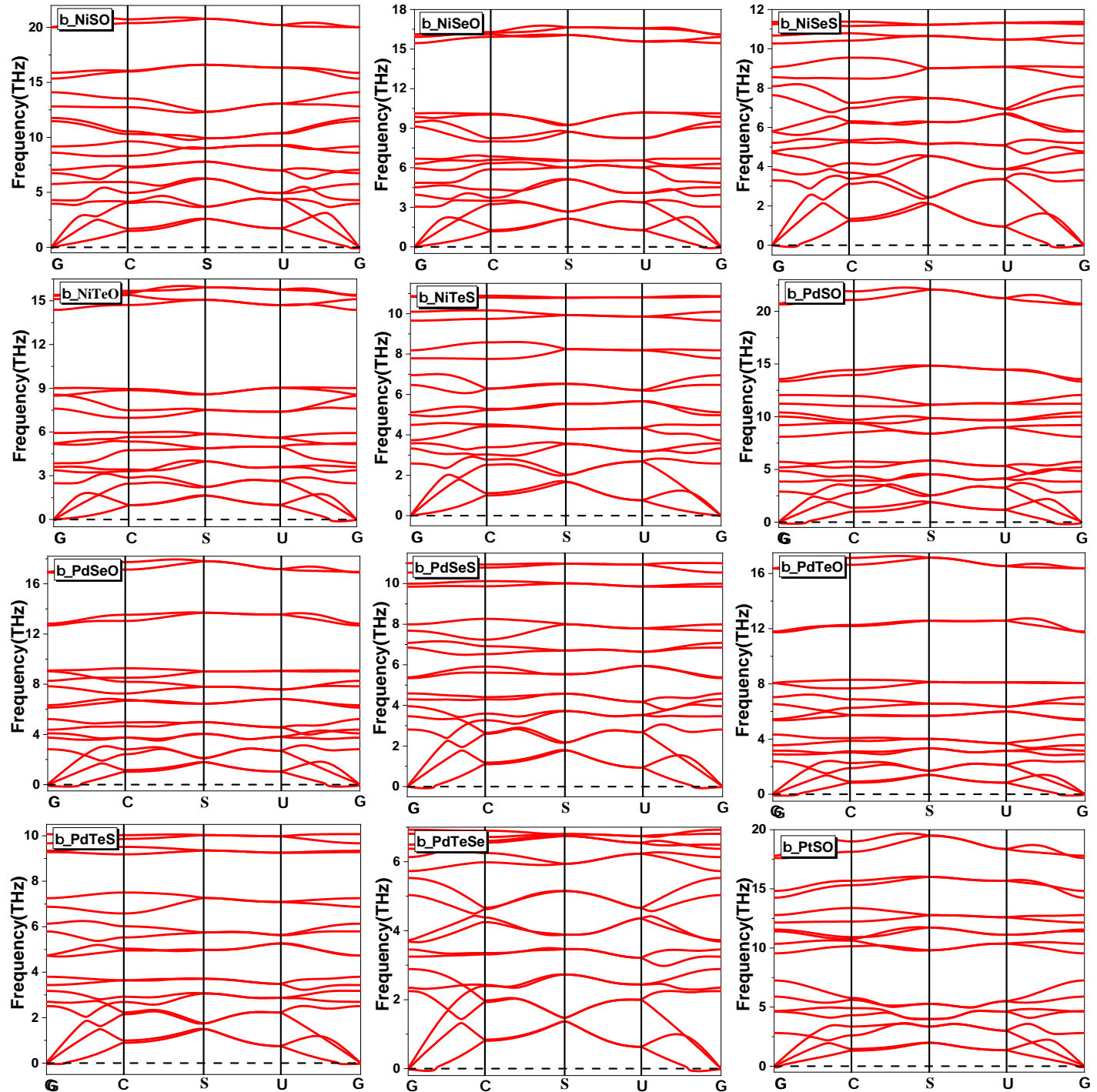
<sup>b</sup>International Center for Computational Method & Software, Jilin University, Changchun, 130012, China.

<sup>c</sup>International Center of Future Science, Jilin University, Changchun 130012, China.

<sup>d</sup>College of Materials Science and Engineering, Jilin University, Changchun 130012, China.

<sup>e</sup>Key Laboratory of Physics and Technology for Advanced Batteries (Ministry of Education), Jilin University, Changchun, 130012, China.

## 2 The phonon spectrum of 2D MXY phase



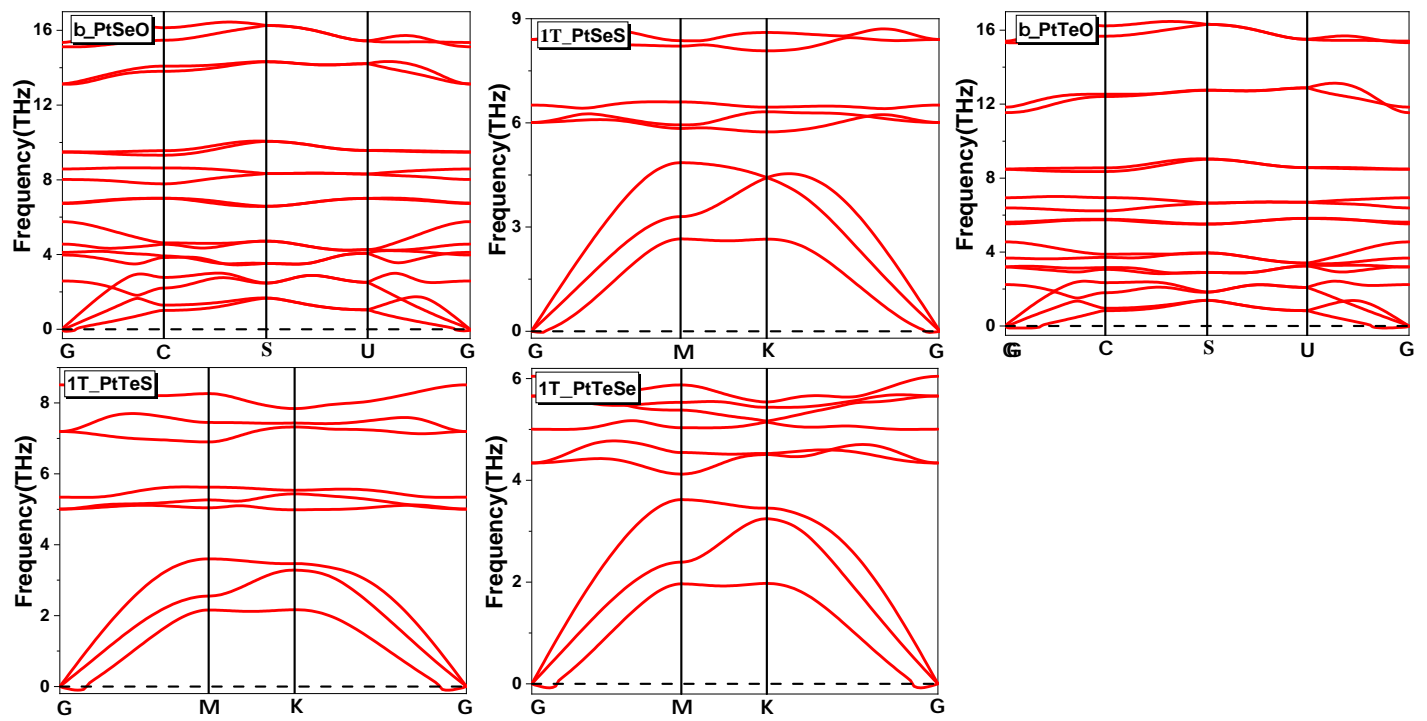


Fig. S2 The calculated phonon dispersions for 2D MXY.

### 3 The mechanical stability of the stable 2D MXY phases

We calculated the orientation dependent Poisson's ratio  $v(\theta)$  and Young's modulus  $Y(\theta)$  for the lowest energy phase in NiXY, PdXY and PtXY monolayers by using the following equations<sup>1</sup>.

$$Y(\theta) = \frac{C_{11}C_{22} - C_{12}^2}{C_{11}\sin^4(\theta) + A\sin^2(\theta)\cos^2(\theta) + C_{22}\cos^4(\theta)} \quad (1)$$

$$v(\theta) = \frac{C_{12}\sin^4(\theta) - B\sin^2(\theta)\cos^2(\theta) + C_{12}\cos^4(\theta)}{C_{11}\sin^4(\theta) + A\sin^2(\theta)\cos^2(\theta) + C_{22}\cos^4(\theta)} \quad (2)$$

where  $A = (C_{11}C_{22} - C_{12}^2)/C_{66}$  -  $2C_{12}$  and  $B = C_{11} + C_{22} - (C_{11}C_{22} - C_{12}^2)/C_{66}$ .

Table S2 Calculated elastic constants ( $C_{11}$ ,  $C_{22}$ ,  $C_{12}$ ,  $C_{66}$ , in  $N m^{-1}$ ), Young's modulus ( $Y_x$ ,  $Y_y$ : the Y value along the x, y direction, in  $N m^{-1}$ ), and Poisson's ratio ( $v_x$ ,  $v_y$ ) of the stable 2D NiXY, PdXY and PtXY phases.

Materials	$C_{11}$	$C_{22}$	$C_{12}$	$C_{66}$	$Y_x$	$Y_y$	$v_x$	$v_y$
$\beta$ _NiSO	112.06	110.66	19.15	30.47	108.74	107.39	0.17	0.17
$\beta$ _NiSeO	100.91	97.44	19.35	28.20	97.07	93.73	0.20	0.19
$\beta$ _NiSeS	81.96	47.22	-0.89	29.28	81.94	47.21	-0.02	-0.01
$\beta$ _NiTeO	86.25	78.32	18.21	24.77	82.02	74.48	0.23	0.21
$\beta$ _NiTeS	72.35	35.45	-1.30	27.23	72.31	35.43	-0.04	-0.02
$\beta$ _PdSO	75.23	80.59	6.05	20.01	74.77	80.11	0.08	0.08
$\beta$ _PdSeO	74.68	65.61	5.62	18.64	74.19	65.18	0.09	0.08
$\beta$ _PdSeS	69.39	46.14	2.04	21.50	69.30	46.08	0.04	0.03
$\beta$ _PdTeO	65.42	49.08	5.32	15.60	64.84	48.65	0.11	0.08
$\beta$ _PdTeS	60.97	34.56	0.92	19.52	60.94	34.55	0.03	0.02
$\beta$ _PdTeSe	55.06	0.48	28.65	18.33	55.04	28.64	0.02	0.01
$\beta$ _PtSO	107.29	104.03	12.25	24.41	105.85	102.63	0.12	0.11
$\beta$ _PtSeO	93.90	79.99	10.34	22.18	92.57	78.85	0.13	0.11
1T_PtSeS	77.43	77.43	20.45	28.49	72.03	72.03	0.26	0.26
$\beta$ _PtTeO	77.63	55.19	8.22	18.71	76.40	54.32	0.15	0.11
1T_PtTeS	64.97	64.97	17.23	23.87	60.40	60.40	0.27	0.27
1T_PtTeSe	64.99	64.99	17.73	23.63	60.15	60.15	0.27	0.27

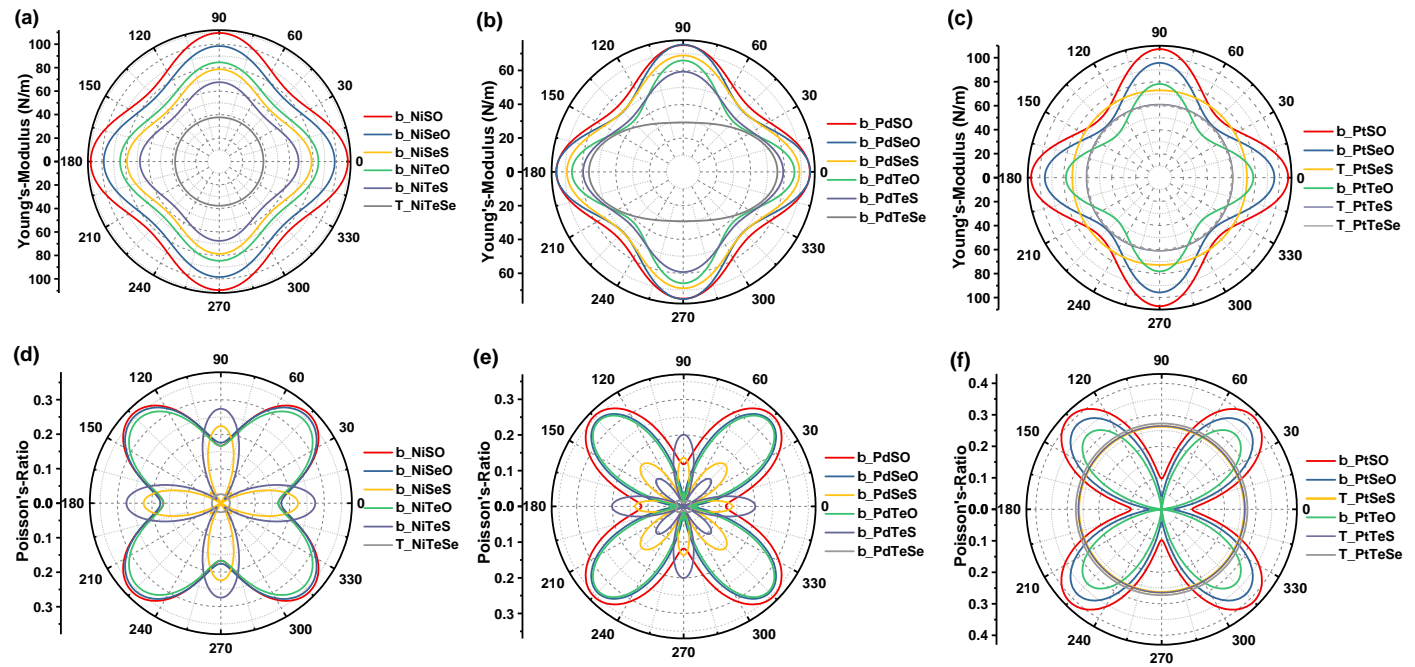


Fig. S3 Calculated orientation-dependent Young's modulus ( $Y(\theta)$ ) (upper panels) and Poisson's ratio ( $v(\theta)$ ) (lower panels)

#### 4 The electronic localization function (ELF) for 2D TMXY

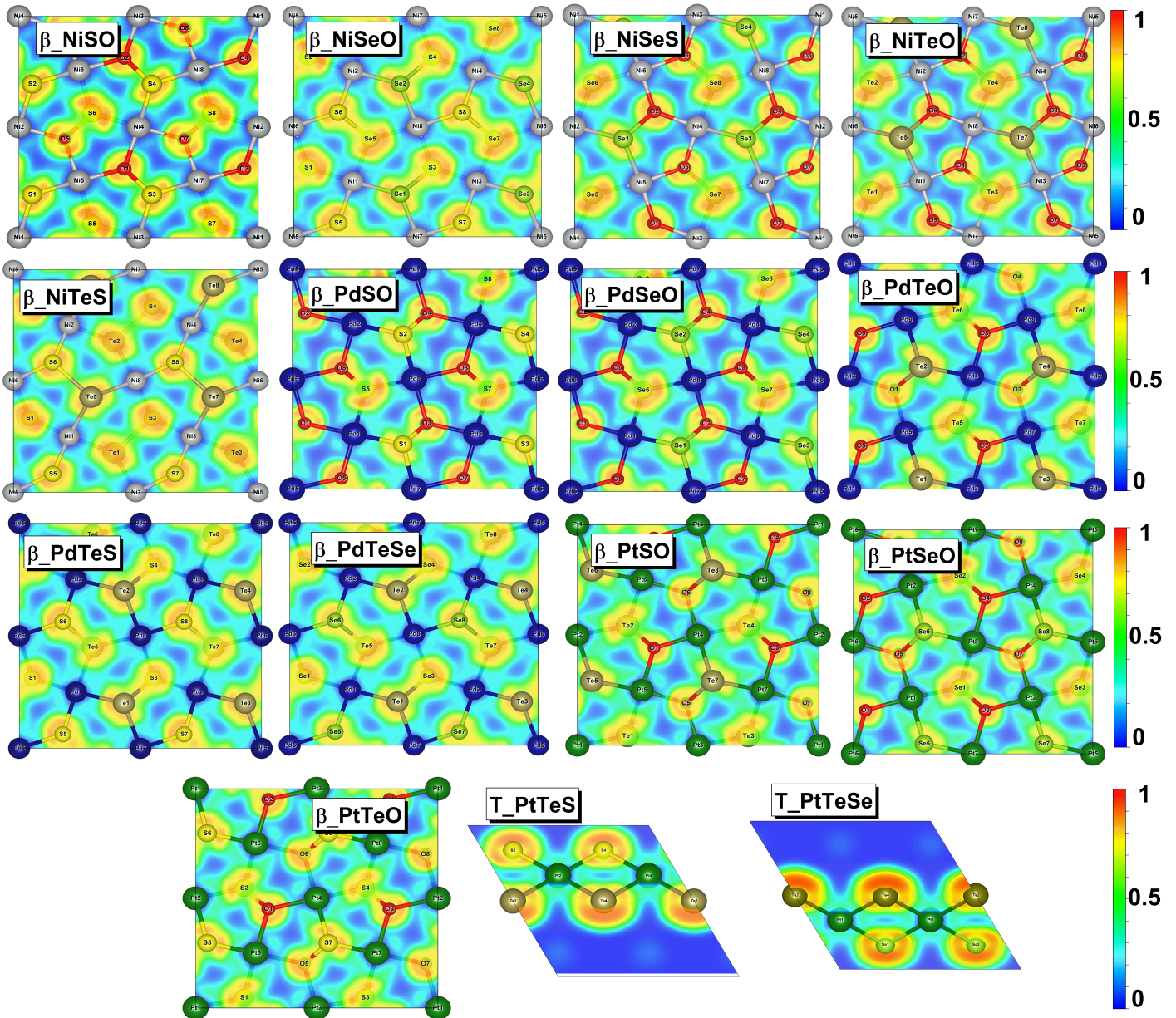
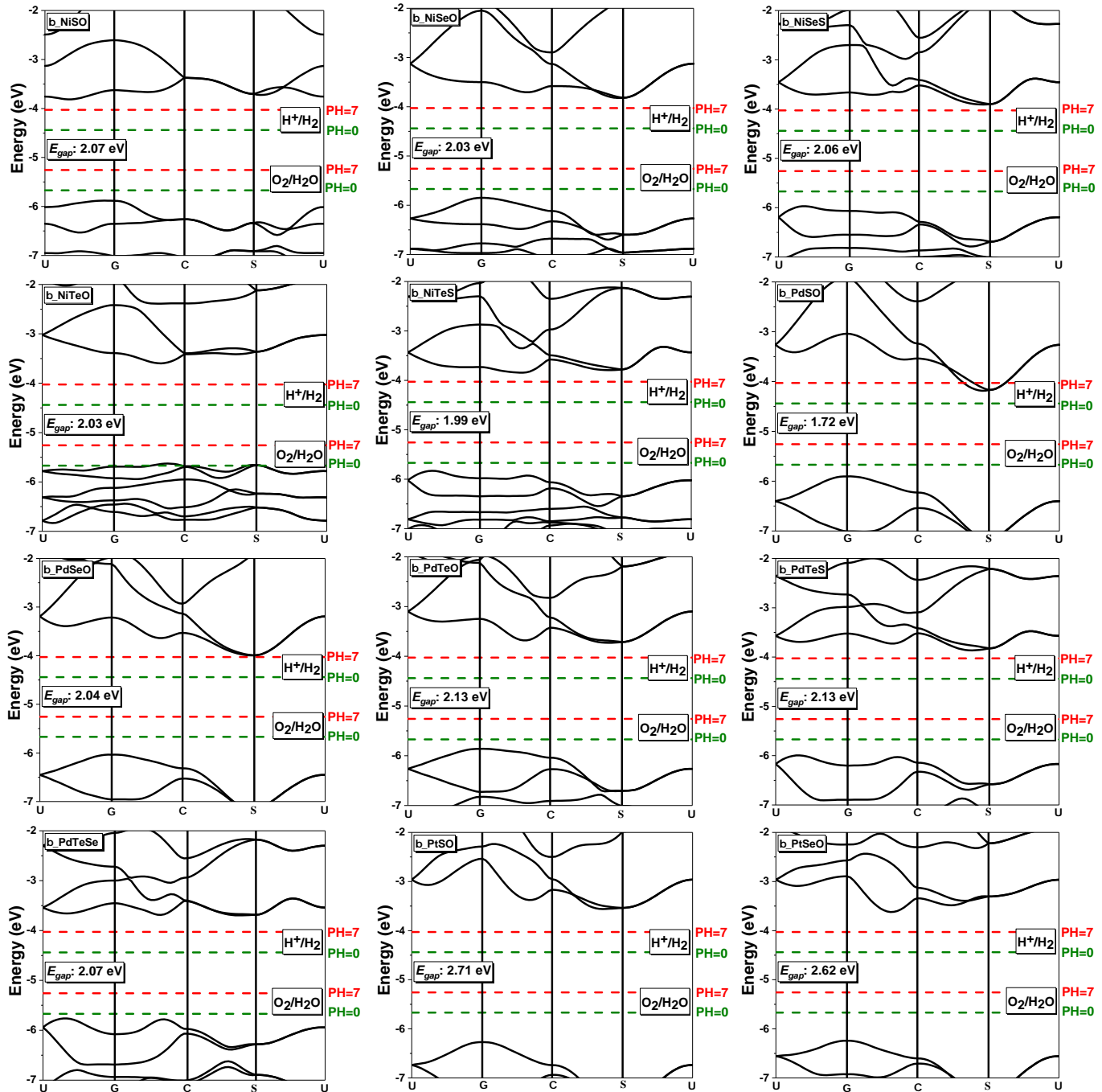


Fig. S4 The electronic localization function (ELF) for 2D MXY monolayers. In the ELF maps, the red and blue colors refer to the highest value (1.00) and the lowest value (0.00) of ELF, respectively. Corresponding to the accumulation and depletion of electrons in the two colored regions.

## 5 The HSE band structures of 2D MXY



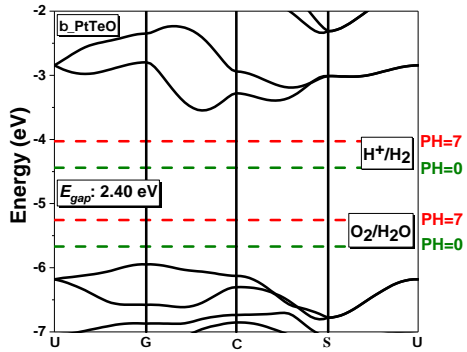


Fig. S5 The HSE band structures of MXY monolayer. The energy level positions have been corrected by vacuum level. The water redox potentials at pH = 0/7 are marked by the green/red dotted lines.

## 6 Convergence test for Optical property and band gap of 2D MXY

We choose the PdTeSe monolayer to examine the convergence of the GW calculations using the VASP code<sup>2</sup>, especially for the energy cutoff of the response functions  $E_\epsilon$ , the number of empty states N and k-grid. It is obvious that N = 600,  $E_\epsilon$  = 200 eV and k-grid is  $11 \times 11 \times 1$  are enough to converge the band gap within 0.02 eV. We Use the VASP code to calculate the optical properties of all MXY materials.

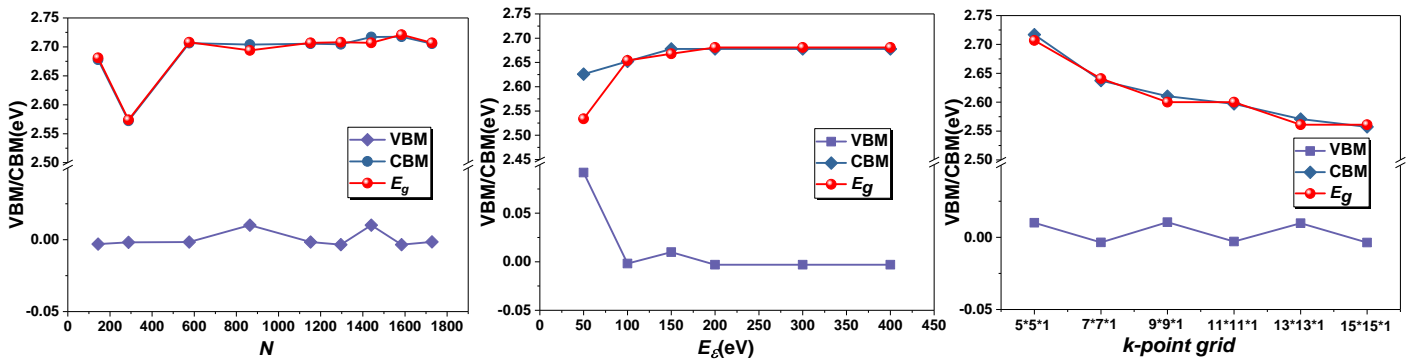
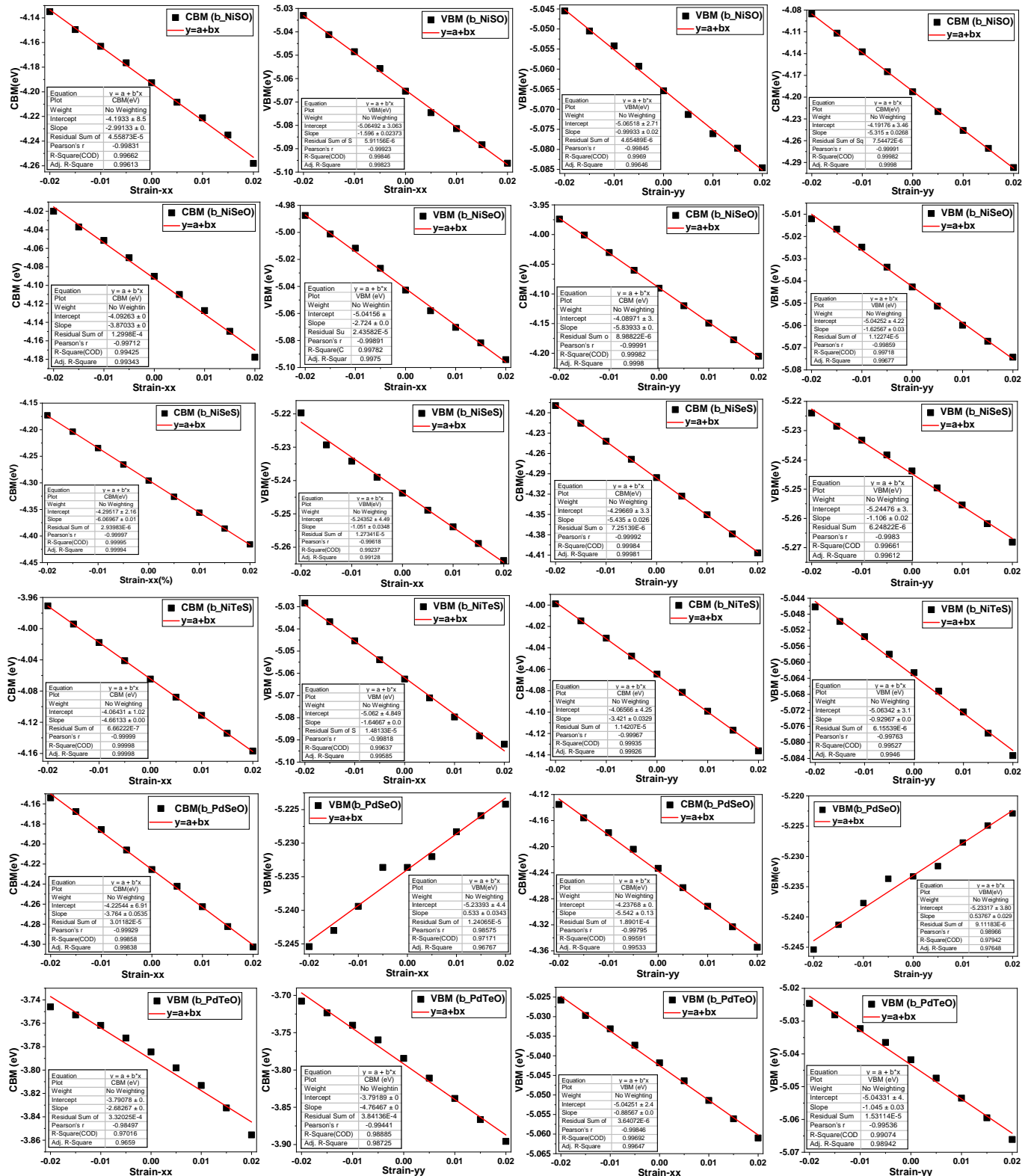


Fig. S6 Convergence of the band energy and band gap of the 2D PdTeSe monolayer with respect to the number of empty states N, the energy cutoff of the response function  $E_\epsilon$  and k-point grid. Absorption spectra  $A(\omega)$  calculated by GW-BSE using the VASP software.

Table S3 Band Gaps at PBE level ( $E_{\text{PBE}}$ ), Band Gaps Based on HSE06 ( $E_{\text{HSE}}$ ), Direct Band Gaps Based on  $G_0W_0$  ( $E_{G_0W_0}^{\text{d}}$ ) and Indirect Band Gaps Based on  $G_0W_0$  ( $E_{G_0W_0}^{\text{id}}$ ) and Optical Band Gaps  $E_{\text{opt}}$ , Exciton Binding Energies ( $E_b$ ). The band gaps are given in eV.

Materials	$E_{\text{PBE}}$	$E_{\text{HSE}}$	$E_{G_0W_0}^{\text{d}}$	$E_{G_0W_0}^{\text{id}}$	$E_{\text{opt}}$	$E_b$
$\beta$ _NiSO	0.89	2.07	1.78	1.62	1.01	0.77
$\beta$ _NiSeO	0.95	2.03	1.61	1.55	0.99	0.62
$\beta$ _NiSeS	0.94	2.06	1.76	1.61	1.40	0.36
$\beta$ _NiTeS	1.02	1.99	1.53	1.37	1.36	0.17
$\beta$ _PdSeO	1.02	2.04	2.71	2.29	2.12	0.59
$\beta$ _PdTeO	1.22	2.13	2.30	2.22	1.67	0.64
$\beta$ _PdTeS	1.23	2.13	2.34	2.29	1.84	0.51
$\beta$ _PdTeSe	1.37	2.07	2.15	2.10	1.72	0.43
$\beta$ _PtSO	1.51	2.71	3.50	2.97	2.84	0.66
$\beta$ _PtSeO	1.57	2.62	3.01	2.74	2.45	0.56
$\beta$ _PtTeO	1.49	2.4	2.51	2.40	1.95	0.56

## 7 Mobility of photoexcited Carriers and fitting the deformation potential constant $E_i$ for 2D MXY



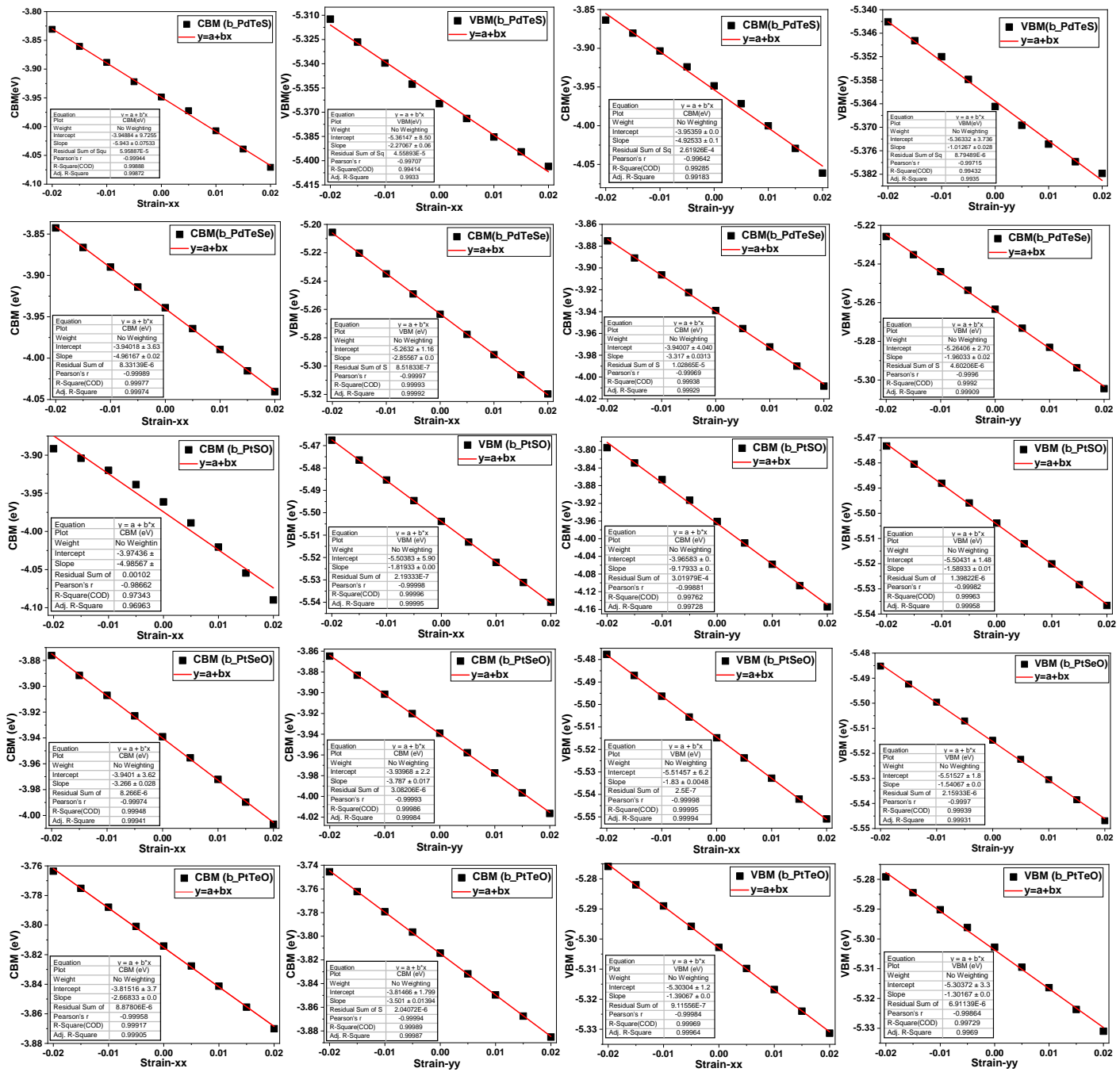


Fig. S7 Fitting the deformation potential constant  $E_i$  for monolayer MXY: x axis uniaxial strained CBM, y axis uniaxial strained CBM, x axis uniaxial strained VBM and y axis uniaxial strained VBM.

Table 4 The Effective Mass ( $m^*$ ) of electrons and holes, Elastic Modulus ( $C_{2D}$ ), Deformation Potential Constant  $E_i$ , and Carrier Mobility ( $\mu$ ) along x and y Directions for these 2D MXY monolayers.

Materials	Carrier type	$m^*/m_0$	$C_{2D}(Jm^{-2})$	$E_i$	$\mu (cm^2V^{-1}s^{-1})$
$\beta\text{-NiSO}$	e(x)	0.96	107.61	2.99	251.02
	h(x)	0.88	107.61	1.60	811.04
	e(y)	1.17	106.46	1.00	1826.27
	h(y)	1.84	106.46	5.32	34.41
$\beta\text{-NiSeO}$	e(x)	1.43	96.42	3.87	84.33
	h(x)	2.16	96.42	2.72	85.20
	e(y)	0.91	92.98	5.84	56.35
	h(y)	1.04	92.98	1.63	479.81
$\beta\text{-NiSeS}$	e(x)	0.55	81.53	6.07	86.33
	h(x)	1.03	81.53	1.05	1481.86
	e(y)	1.78	47.09	5.44	19.38
	h(y)	0.94	47.09	1.11	895.23
$\beta\text{-NiTeS}$	e(x)	0.37	71.93	4.66	231.81
	h(x)	1.25	71.93	1.65	459.00
	e(y)	1.82	35.07	3.42	42.76
	h(y)	0.79	35.07	0.93	1109.13
$\beta\text{-PdSeO}$	e(x)	0.56	72.70	3.76	264.21
	h(x)	2.20	72.70	0.53	1472.75
	e(y)	1.00	64.37	5.54	59.87
	h(y)	1.29	64.37	0.54	2179.51
$\beta\text{-PdTeO}$	e(x)	1.01	63.91	2.68	106.10
	h(x)	2.78	63.91	4.76	11.89
	e(y)	3.11	48.09	4.93	237.87
	h(y)	1.19	48.09	1.01	435.58
$\beta\text{-PdTeS}$	e(x)	0.58	60.52	5.94	71.31
	h(x)	1.17	60.52	2.27	238.55
	e(y)	1.32	34.32	4.93	25.85
	h(y)	0.69	34.32	1.01	1149.09
$\beta\text{-PdTeSe}$	e(x)	0.65	54.83	4.96	84.20
	h(x)	1.39	54.83	2.86	111.42
	e(y)	1.19	28.41	3.32	53.04
	h(y)	0.63	28.41	1.96	271.16
$\beta\text{-PtSO}$	e(x)	0.55	104.21	4.98	146.46
	h(x)	1.09	104.21	1.82	610.79
	e(y)	2.29	101.76	9.18	10.09
	h(y)	0.95	101.76	1.59	893.44
$\beta\text{-PtSeO}$	e(x)	0.43	93.29	3.27	529.53
	h(x)	1.05	93.29	3.79	124.36
	e(y)	1.61	79.24	1.83	379.25
	h(y)	1.07	79.24	1.54	626.70
$\beta\text{-PtTeO}$	e(x)	0.38	75.78	2.67	1073.75
	h(x)	1.57	75.78	3.50	62.80
	e(y)	0.82	54.07	1.39	1303.36
	h(y)	1.15	54.07	1.30	443.69

## 8 Solar driven water splitting processes on 2D MXY

The thermodynamics of water splitting on 2D MXY monolayers are estimated by examining the HER and OER processes, respectively. We marked \*, H\*, OH\*, O\*, OOH\* as the bare surface and HER, OER intermediates adsorbed on the 2D MXY monolayers.

The overall hydrogen evolution reaction under standard conditions can be described as follows:



While for OER, the four-electron process is interpreted as following four elementary steps:



For each reaction of both oxidation and hydrogen production, the free energy different under the effect of pH and an extra potential bias can be written as:

$$\Delta G = \Delta E + \Delta ZPE - T \Delta S + \Delta G_{pH} + \Delta G_U \quad (9)$$

The  $\Delta E$ ,  $\Delta ZPE$ , and  $\Delta S$  are the different energy, zero-point energy, and entropy of the reaction, respectively. The  $\Delta E$  is obtained from DFT calculation, while the  $\Delta ZPE$ , and  $\Delta S$  are calculated form the values of Table S3. The entropies of free molecules can be found from the NIST database. As the DFT method cannot accurately describe the high-spin ground state of the O<sub>2</sub> molecule, the Gibbs free energy of O<sub>2</sub> [ $G_{O_2}$ ] is obtained by  $G_{O_2} = 2G_{H_2O} - 2G_{H_2} + 4.92$ .  $T$  represents indoor temperature in this work.  $\Delta G_{pH}$  ( $\Delta G_{pH} = k_B T \times \ln 10 \times \text{pH}$ ) represents the free energy contributed in different pH concentration.  $\Delta G_U$  ( $\Delta G_U = -eU$ ) denotes extra potential bias provided by an electron in the electrode, where  $U$  is the electrode potential relative to the standard hydrogen electrode (SHE).  $\Delta G_U$  refers to the Gibbs free energy change imposed by light-induced driven potential ( $U$ ) and equals to  $-eU$ . The light-induced driven potential for HER can be obtained by  $U_e = [E_{CBM} - (-4.44 + 0.059 \times \text{pH})]/e$ , and the driven potential for OER is determined by  $U_h = [-E_{VBM} + (-4.44 + 0.059 \times \text{pH})]/e$ .  $E_{VBM}$  and  $E_{CBM}$  represents the energy level of valance band maximum (VBM) and conduction band minimum (CBM) of the photocatalysts, respectively. Both of the VBM and CBM were regulated by the vacuum level.

$$\Delta G_3 = G_{H*} - \frac{1}{2}G_{H_2} - G_* + \Delta G_U + \Delta G_{pH} \quad (10)$$

$$\Delta G_4 = G_* + \frac{1}{2}G_{H_2} - G_{H*} + \Delta G_U + \Delta G_{pH} \quad (11)$$

$$\Delta G_5 = G_{OH*} + \frac{1}{2}G_{H_2} - G_* - G_{H_2O} + \Delta G_U - \Delta G_{pH} \quad (12)$$

$$\Delta G_6 = G_{O*} + \frac{1}{2}G_{H_2} - G_{OH*} + \Delta G_U - \Delta G_{pH} \quad (13)$$

$$\Delta G_7 = G_{OOH*} + \frac{1}{2}G_{H_2} - G_{O*} - G_{H_2O} + \Delta G_U - \Delta G_{pH} \quad (14)$$

$$\Delta G_8 = G_* + \frac{1}{2}G_{H_2} + G_{O_2} - G_{OOH*} + \Delta G_U - \Delta G_{pH} \quad (15)$$

Table S5 Values used for the entropy and zero-point energy corrections in determining the free energy of reactants, products, and intermediate species adsorbed on catalysts<sup>3</sup>.

Species	$T \times S$ (eV)	ZPE (eV)
H*	0	0.17
O*	0.06	0.07
OH*	0.08	0.33
OOH*	0.21	0.43
H <sub>2</sub> (g)	0.41	0.27
H <sub>2</sub> O(g)	0.58	0.57

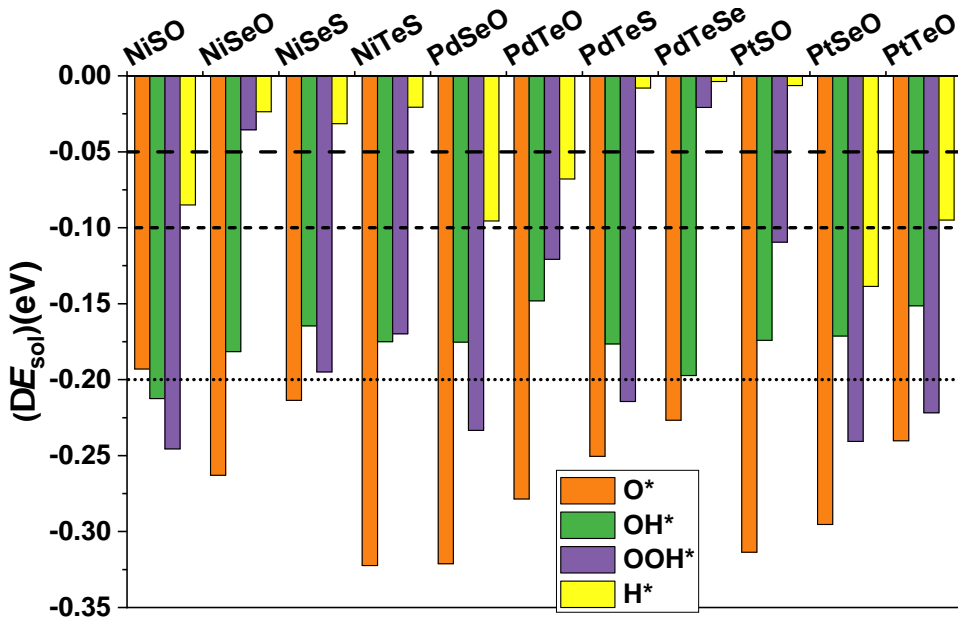


Fig. S8 Adsorption solvation energies for several adsorbates on the MXY monolayers calculated by using VASPsol. The unit of the adsorption solvation energies is eV. The dashed line at -0.05, -0.1 and -0.2 eV indicate the weak, moderate and strong solvation effect suggested by Deskins et al<sup>4</sup>.

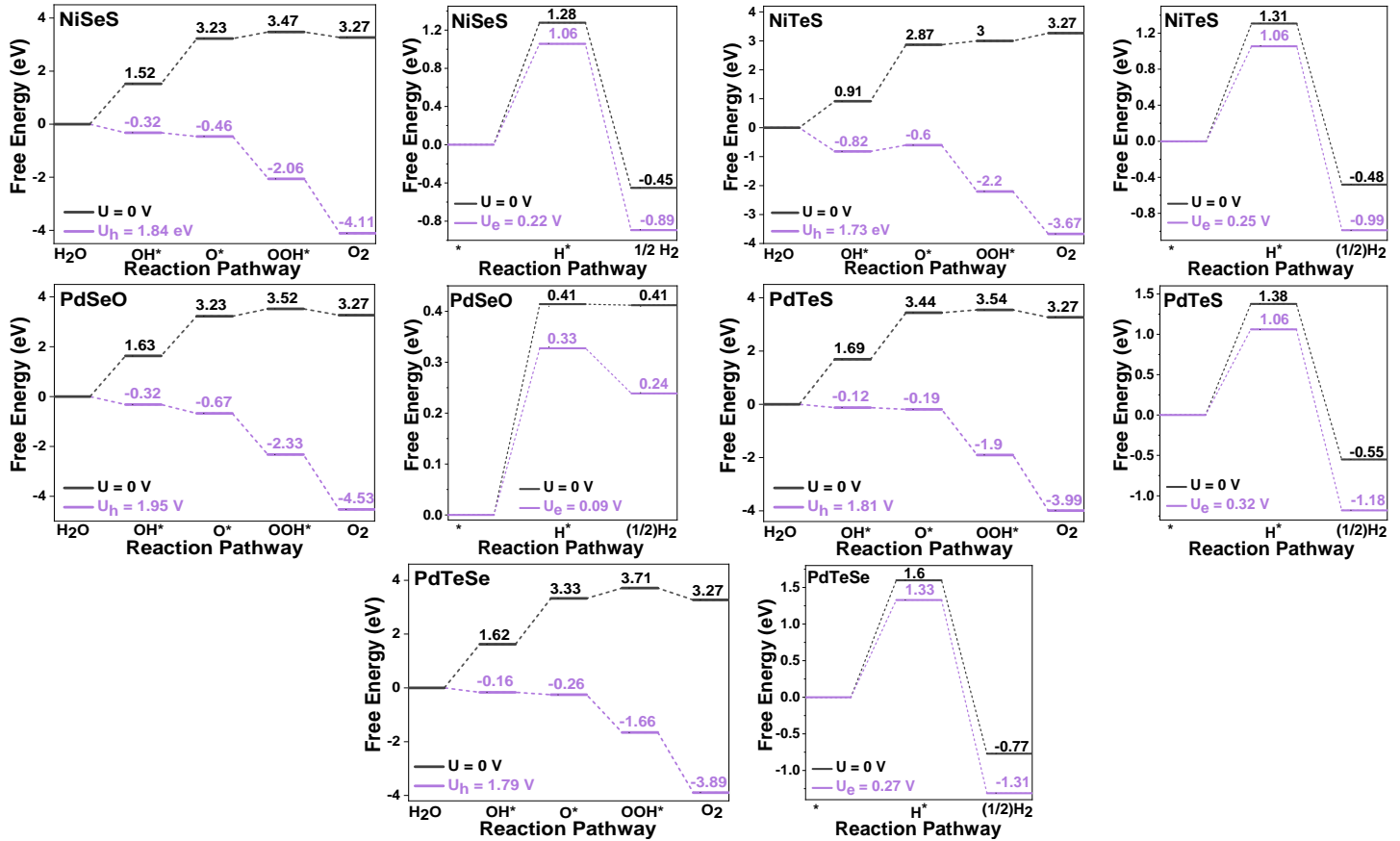


Fig. S9 Gibbs free energy ( $\Delta G$ ) vs. reaction coordinate for water oxidation and hydrogen reduction half reactions in MXy applied at pH = 7 under different potentials including solvation effects in an aqueous solution. The value of  $\Delta G$  in each elementary step is also shown.  $U_h$  and  $U_e$  are potentials provided by photogenerated holes for water oxidation reduction and photogenerated electrons for hydrogen reduction, respectively.

## Notes and references

- 1 E. Cadelano, P. L. Palla, S. Giordano and L. Colombo, *Phys. Rev. B*, 2010, **82**, 235414.
- 2 G. Kresse and J. Hafner, *Phys. Rev. B: Condens. Matter Mater. Phys.*, 1993, **47**, 558–561.
- 3 H. Xu, D. Cheng, D. Cao and X. C. Zeng, *Nat. Catal.*, 2018, **1**, 339–348.
- 4 S. K. Iyemperumal and N. A. Deskins, *Chemphyschem*, 2017, **18**, 2171–2190.